Optoelectronic time-domain characterization of a 100 GHz sampling oscilloscope

H. Füser [a)*], S. Eichstädt [b)], K. Baaske [a)], C. Elster [b)], K. Kuhlmann [a)], R. Judaschke [a)], K. Pierz [a)], and M. Bieler [a)]

[a)] *Physikalisch-Technische Bundesanstalt, Bundesallee 100, D-38116 Braunschweig, Germany*

[b)] *Physikalisch-Technische Bundesanstalt, Abbestraße 2-12, D-10587 Berlin, Germany*

Abstract

We have performed an optoelectronic measurement of the impulse response of an ultrafast sampling oscilloscope with a nominal bandwidth of 100 GHz within a time window of approximately 100 ps. Our experimental technique also considers frequency components above the cut-off frequency of higher-order modes of the 1.0 mm coaxial line, which is shown to be important for the specification of the impulse response of ultrafast sampling oscilloscopes. Additionally, we have measured the reflection coefficient of the sampling head induced by the mismatch of the sampling circuit and the coaxial connector which is larger than 0.5 for certain frequencies. The uncertainty analysis has been done using the Monte Carlo method of Supplement 1 to the 'Guide to the Expression of Uncertainty in Measurement' and correlations in the estimated impulse response have been determined. Our measurements extend previous work which deals with the characterization of 70 GHz oscilloscopes and the measurement of 100 GHz oscilloscopes up to the cut-off frequency of higher-order modes.

---

* Author to whom all correspondence should be addressed;
electronic mail: heiko.fueser@ptb.de

1. Introduction

Ultrafast sampling oscilloscopes with a nominal bandwidth of up to 100 GHz mark the state of the art of today's commercially available high-speed instrumentation. Such oscilloscopes being portable, easy to use, and relatively inexpensive are ideal characterization instruments for a variety of applications [1,2], in particular, for the measurement of digital signals [3-5]. However, when using sampling oscilloscopes for the measurement of ultrafast signals, it is important to know the oscilloscope's impulse response since it may significantly distort the time traces to be measured. With the knowledge of the oscilloscope's impulse response, linear response theory can be employed to reconstruct the undistorted signal from the oscilloscope time trace. In order to reliably measure the impulse response of an oscilloscope it is essential to use a measurement technique with a bandwidth that is considerably larger than the one of the oscilloscope under test. This is demonstrated by analyzing the time trace of a fast electrical signal measured with a 100 GHz sampling oscilloscope, see Fig. 1. The corresponding Fourier transform of the time-domain signal is plotted in the inset of Fig. 1 and visualizes that the oscilloscope is capable to measure frequency components of up to ~190 GHz. This also implies that for the measurement of very broadband electrical signals, sampling oscilloscopes have to be characterized even beyond the regular monomode operating bandwidth of coaxial line systems, which is 110 GHz for the 1.0 mm coaxial system as employed in 100 GHz sampling heads.

Optoelectronic techniques, in combination with femtosecond lasers, are well suited for the characterization of ultrafast sampling oscilloscopes, mainly due to their unmatched measurement bandwidth that even exceeds 1 THz [6]. The time and frequency axis of such techniques is traceable to the SI units. Currently three NMIs (PTB [7] and NPL [8] in Europe and NIST [9] in the USA) have established optoelectronic measurement techniques for the characterization of sampling oscilloscopes. In recent years a single parameter characterization, i.e., the measurement of the rise time of the step response [10], has been extended to waveform metrology where the uncertainty of each time (or frequency) step can be specified [7,11-13]. NIST uses an approach that combines time-based electro-optic sampling with frequency-based VNA measurements. A frequency increment of only

200 MHz with degraded uncertainty from DC to 1 GHz [14] is achieved, yet, with an upper frequency limit of 110 GHz [9]. This approach constitutes the state-of-the-art technique for the characterization of ultrafast sampling oscilloscopes in the low frequency range. However, it is not an appropriate method for a full time-domain characterization, see Fig. 1.

In this paper, we present measurements of the impulse response of a 100 GHz sampling oscilloscope within a measurement window of 100 ps. Although our measurement technique does not yield the frequency resolution presented in [9], it captures the time-domain response including frequencies above the cut-off frequency of higher-order modes of the coaxial waveguide. This is a prerequisite to derive a time-domain representation of the oscilloscope's response, i.e., the impulse or step response. The uncertainty analysis is based on a Monte Carlo method according to Supplement 1 to the 'Guide to the Expression of Uncertainty in Measurement' (GUM-S1) [15]. This paper extends previous work [16] in three main points: (i) The whole measurement technique is extended to 1.0 mm coaxial waveguides, including the measurement of the impulse response of a 1.0 mm coaxial-coplanar microwave probe. (ii) The reflection coefficient (mismatch) of the oscilloscope is directly measured. (iii) The uncertainty analysis determines correlations in the estimate of the impulse response arising from the analytical model.

The remainder of this paper is structured as follows. In Sec. 2 the experimental set-up is described together with the data analysis and the evaluation of uncertainties. The characterization of the 1.0 mm microwave probe is discussed in Sec. 3 before the measurement of the impulse response of the oscilloscope and its mismatch is presented in Sec. 4. Section 5 finishes with a summary and an outlook.

2. Experimental setup, model for data analysis, and uncertainty evaluation

The characterization of the time response of the oscilloscope is based on femtosecond optoelectronic methods. Broadband (>300 GHz bandwidth) electrical test pulses are generated using a photoconductive switch (PCS), which is embedded in a coplanar waveguide (CPW), see Fig. 2. The CPW consists of a 30 µm broad signal stripe separated by 20 µm from two 500 µm ground stripes evaporated onto

low temperature grown GaAs (LT-GaAs, carrier life time ~1 ps). The characteristic impedance of this structure is close to 50 Ω [17]. The excitation gap in the center conductor is 10 µm long and biased with 20 V. For the simultaneous generation and detection of ultrashort voltage pulses with laser pulses of the same wavelength we employ the technique discussed in Ref. [6]. A femtosecond laser (Coherent Mira, 76 MHz repetition rate) emits 150 fs long pulses with a center wavelength of approximately 900 nm. The laser beam is split into a pump and probe beam. The pump beam is focused on the photoconductive gap. At a wavelength of ~900 nm the absorption in the LT-GaAs material is, on the one hand, large enough to generate sufficient carriers [6], whose movement induces a voltage pulse. The probe beam is focused on the LT-GaAs material right between the center stripe and one ground stripe, see Fig. 2. The absorption at ~900 nm is, on the other hand, small enough to allow a significant part of the laser beam to propagate through the substrate and produce an electro-optic (EO) signal in the detector which is proportional to the electric field of the voltage pulses. With a mechanical delay line in the probe beam path, time-discrete sampling can be performed and a waveform measurement of the current pulses traveling on the CPW is possible. Calibrating the mechanical delay line, the time axis of the measurement is traceable to the unit of length, and, thus to the unit of time.

To transfer the ultrashort voltage pulses from the CPW to the oscilloscope, a commercial 1.0 mm, 50 Ohm microwave probe (MWP, Picoprobe 110H-GSG-50-P) is used. The oscilloscope input is directly connected to the coaxial end of the MWP. The MWP is attached to the center of the CPW with a distance of 5 mm to both the photoconductive switch and the end of the CPW. Hence, the MWP and the CPW form a T-junction. We use the T-junction instead of attaching the MWP to an abrupt end of the CPW since this arrangement offers the largest flexibility. For example, contacting the end of the CWP with bond wires allows us to measure the amplitude of the cw photocurrent being an indication of how good the pump beam is focused on the photoconductive gap. The voltage pulses are measured right at this T-junction which has several advantages as discussed in the next paragraph. Since the whole experimental arrangement is symmetric with respect to the ground line only even coplanar waveguide modes are excited. This has been verified by comparing two

voltage pulses measured with the probe beam being focused on both gaps between the center line and the two ground lines. Moreover, the EO measurements were performed over a limited time window of approximately 100 ps in order to avoid distortions caused by reflections at both ends of the CPW [6]. Although the inclusion of reflections does not lead to a fundamental problem, it significantly complicates the data analysis. Except for the type of microwave probe the setup is identical to the one discussed in Ref. [6].

Measuring the voltage pulses directly at the T-junction yields the pulses $v_{\mathrm{eos}}(t)$ which are transmitted from the CPW into the MWP. Thus, in order to determine the pulses at the input connector of the oscilloscope, which is connected to the coaxial end of the MWP, one has to convolve $v_{\mathrm{eos}}(t)$ with the impulse response of the MWP, $h_{\mathrm{probe}}(t)$ [18]. The measured oscilloscope trace $v_{\mathrm{osc}}(t)$ has then to be deconvolved with the voltage pulse at the oscilloscope's input connector to obtain the impulse response of the oscilloscope $h_{\mathrm{osc}}(t)$. The trigger signal for the oscilloscope is obtained from a fast photodiode on which a small portion of the laser beam is focused. The resulting voltage pulse has an amplitude of approximately 70 mV and a 3 dB bandwidth of approximately 0.7 GHz. The trigger level of the oscilloscope is set to 40 mV.

Although we perform all measurements in the time domain, in which also the majority of experimental results is specified, the data analysis is carried out in the frequency domain. This is simply because for our particular case convolutions and deconvolutions in the time domain are much easier computed in the frequency domain by performing multiplications and divisions, respectively [19]. To avoid problems arising from the periodicity of the Fast Fourier Transform we usually consider time-domain measurements ranging from 40 ps before the maximum of the voltage pulses to 80 ps after the maximum. This 120 ps time window is then doubled to 240 ps by zero padding. This ensures that signals being present at the end of the 120 ps time traces are negligible small and, thus, do not lead to a distinct signal at the beginning of the time window. When giving results in the frequency domain we only consider the length of the measured time window, i.e., obtain a frequency spacing of 8.3 GHz.

For the transfer function $H_{\mathrm{osc}}(f)$ of the oscilloscope, which is the Fourier transform of the impulse response $h_{\mathrm{osc}}(t)$, we can set up the following equation:

$$H_{osc}(f) = \frac{V_{osc}(f/\gamma_\tau) \cdot e^{-2(\pi \sigma_{eos} \cdot f)^2}}{V_{eos}(f) \cdot H_{probe}(f) \cdot e^{-2(\pi \sigma_{osc} f/\gamma_\tau)^2}} . \qquad (1)$$

Here, V_{osc} is the Fourier transform of the measured oscilloscope trace, V_{eos} is the Fourier transform of the voltage pulse measured via EO sampling at the T-junction, and H_{probe} is the MWP transfer function. The observed oscilloscope trace actually is an average over a large number of sampling points, and therefore can be modeled as a convolution of the undistorted signal and a probability density function (PDF) characterizing the oscilloscope's time jitter within the single traces [20]. For the jitter PDF we employ a normal density with zero mean and standard deviation σ_{osc} determined by additional measurements. Correction of the oscilloscope's averaged trace is then carried out by a deconvolution with the jitter PDF, leading to the third factor in the denominator of Eq. (1). Additionally we include a correction factor γ_τ for the distortion of the oscilloscope's time base [16]. The limited temporal resolution of our EO sampling technique is accounted for by deconvolving the EO signal with a Gaussian impulse response (with parameter σ_{eos}) as expressed through the second term in the numerator of Eq. (1), see Ref. [6]. Knowing all input variables it is straightforward to calculate the impulse response of the oscilloscope using Eq. (1). Note that Eq. (1) is a deconvolution which is in general an ill-posed problem and, thus, requires regularization [21]. To this end, we apply a low-pass filter, see Sec. 4.

With regard to the model used for the data analysis we like to comment on higher-order modes in the 1.0 mm coaxial line, which usually arise from asymmetries in the waveguide such as bends or debris. One usually avoids higher-order modes since deleterious effects may arise due to the superposition of modes with different propagation constants. Moreover their excitation cannot be controlled and it is difficult to repeat the result. We have avoided any waveguide asymmetries and repeated the experiments several times. Thus we are confident that - even if higher-order modes were excited - their influence is covered by our uncertainty analysis.

The uncertainty evaluation is performed by a Monte Carlo method according to GUM-S1 [15]. To this end, a (joint) PDF $p_{\mathbf{x}}(\xi)$ is assigned to the input quantities $\mathbf{x}$, i.e., the quantities on the right-hand side of Eq. (1), that represent the state of knowledge about their values. This PDF is then propagated through Eq. (1) to obtain a PDF for the output quantity $\boldsymbol{H}^{\mathrm{T}} = (H(f_1),...,H(f_N))^{\mathrm{T}}$, with N being the number of data points in the measured time traces. This requires one to assign a (joint) PDF for

$$\begin{aligned}\boldsymbol{x}^{\mathrm{T}} = (&\sigma_{eos}, \sigma_{osc}, \gamma_t, h_{probe}(t_1),...,h_{probe}(t_N),\\ &v_{eos}(t_1),...,v_{eos}(t_N), v_{osc}(t_1),...,v_{osc}(t_N))^{\mathrm{T}}.\end{aligned} \tag{2}$$

From these input quantities – given in the time domain – the frequency response is calculated using the discrete Fourier transform and Eq. (1). The impulse response $h_{\mathrm{osc}}(t)$ is then obtained by an inverse Fourier transform of the frequency response.

We assume knowledge about the input quantities has been obtained independently. Thus, the joint PDF $p_{\mathbf{x}}(\xi)$ is the product of the PDFs associated with the individual input quantities. According to Ref. [15] the individual PDFs assigned to the input quantities model the state of knowledge about their values, see Secs. 3 and 4. Hence, a scaled and shifted t-distribution is assigned when knowledge is available by means of a series of indications which are assumed to be drawn independently from a common normal distribution with unknown mean and variance. A normal distribution is assigned when knowledge about the input quantity is available by means of an estimate and its associated uncertainty. To propagate the PDF $p_{\mathbf{x}}(\xi)$ through Eq. (1) a Monte Carlo method is employed as follows. Realizations $\mathbf{x}_k$ for $k = 1,...,M$ are drawn from the PDF $p_{\mathbf{x}}(\xi)$, with the number of drawn samples M being large compared to the number of data points N. For each realization the corresponding value $\mathbf{h}_k^{\mathrm{T}} = (h_{osc}(t_1),...,h_{osc}(t_N))^{\mathrm{T}}$ is calculated from Eq. (1) using the discrete inverse Fourier transform. The realizations $\{\mathbf{h}_1,...,\mathbf{h}_M\}$ represent sample draws from the PDF $p_h(\mathbf{h})$ modeling the state of knowledge about the impulse response $\mathbf{h}^{\mathrm{T}} = (h(t_1),...,h(t_N))^{\mathrm{T}}$. From the samples $\{\mathbf{h}_1,...,\mathbf{h}_M\}$ the estimate (in the sense of quadratic loss) and the (squared standard) uncertainty are computed as

$$\hat{h}(t_i) = \text{mean}_{\,k=1,\ldots,M}\{h_1(t_i),\ldots,h_M(t_i)\}$$
$$U_{\hat{h}} = \text{cov}_{k=1,\ldots,M}\{\mathbf{h}_1^{\mathrm{T}},\ldots,\mathbf{h}_M^{\mathrm{T}}\} \quad . \tag{3}$$

Note that $U_{\hat{h}}$ is a variance-covariance matrix since the measurand is a vector. The diagonal elements $u(\hat{h}(t_1),\hat{h}(t_1)),\ldots,u(\hat{h}(t_N),\hat{h}(t_N))$ are the corresponding squared standard uncertainties.

3. Measurement of the impulse response of the microwave probe

In this section we discuss the measurement of $h_{\text{probe}}(t)$ in detail, since it is inevitably needed to characterize the oscilloscope head, see Eq. (1). In contrast to an approach in which a MWP is characterized in the frequency domain up to 110 GHz [9], we use time-domain EO sampling to obtain $h_{\text{probe}}(t)$. This approach also considers frequencies above the cut-off frequency of higher-order modes of the coaxial line, which is a prerequisite to derive the impulse response of the oscilloscope.

The experimental technique used to determine the impulse response of the 1.0 mm MWP is similar but not identical to the one that we used to characterize a 1.85 mm MWP [17]. The MWP probe is terminated by a coaxial offset short and the voltage pulse traveling into the MWP and the one being reflected from the short are measured at the same position on the CPW. From this reflection the impulse response of the MWP can be determined.

Again, we perform calculations in the frequency domain and derive the transfer function of the microwave probe from:

$$H_{\text{probe}}(f) = \sqrt{\frac{V_{\text{out}}(f)}{V_{\text{in}}(f)\cdot 2R_{\text{junc}}(f)\cdot R_{\text{short}}(f)}} \tag{4}$$

Here, V_{in} and V_{out} are the Fourier transforms of the voltage pulses traveling into the MWP, being reflected and traveling backwards, respectively. Both voltage pulses are directly measured at the T-junction. The reflection coefficient of the offset short is denoted by R_{short}, whereas R_{junc} is the reflection coefficient of CPW/MWP junction for a voltage pulse propagating on the CPW and traveling towards the junction [17]. The reason why H_{probe} depends on R_{junc} is explained in the following. The EO measurement at the T-junction allows us to directly measure the voltage pulse $v_{\text{in}}(t)$ transmitted from the CPW into the MWP. However, the measured voltage pulse

$v_{out}(t)$ traveling in the opposite direction corresponds to the voltage pulse that is transmitted from the MWP onto the CPW and, thus includes the reflection coefficient of the T-junction (for backward traveling pulses). This has to be taken into account when calculating $h_{probe}(t)$.

The deconvolution, Eq. (2), is in general an ill-posed problem and requires regularization. To this end, we apply a low-pass filter (20^{th} order Butterworth filter). The 3 dB bandwidth of the filter is chosen as 250 GHz and is derived from the frequency at which $V_{out}(f)$ approaches the noise level. We assume the regularization error resulting from the application of the low-pass filter to be negligible since the spectral power of $V_{in}(f)$ at the cut-off frequency is three orders of magnitude smaller than at DC.

Three of the four input quantities of Eq. (2) are measured (V_{in}, V_{out}, and R_{junc}) while R_{short} is calculated. We first comment on the EO measurements of the input variables. The voltage pulse $v_{in}(t)$ is obtained from a measurement at the T-junction where the MWP is attached to the CPW, see Fig. 3a. This measurement is repeated with the MWP being removed from the CPW [22]. The measured voltage pulse with attached MWP, $v_{in}(t)$, is composed of two components: the voltage pulse traveling on the CPW towards the T-junction $v_{CPW}(t)$ and the reflection from the junction, $v_r(t)$: $v_{in}(t) = v_{CPW}(t) + v_r(t)$. The additional measurement at the same position without the MWP yields only the voltage pulse $v_{CPW}(t)$. A subtraction of the two time traces allows us to extract $v_r(t)$ and, after a simple division in the frequency domain, the reflection coefficient R_{junc} is obtained: $R_{junc}(f) = V_r(f)/V_{in}(f)$, see Fig. 3b. Over the whole frequency range the reflection coefficient is close to 1/3 which we expect for characteristic impedances of both the microwave probe and the CPW of 50 Ω [17].

For the EO measurement of $v_{out}(t)$ the coaxial end of the MWP is terminated by a coaxial offset short and the measurement epoch is chosen to be long enough (~400 ps), so that the time trace not only includes the voltage pulse propagating into the MWP, $v_{in}(t)$, but also the voltage pulse being reflected from the short and propagating backwards, $v_{out}(t)$. Since the roundtrip time amounts to approximately 240 ps, the reflected and incident pulses can easily be separated. Moreover, we

perform an additional measurement connecting a long coaxial cable instead of the offset short to the coaxial end of the MWP. The cable acts as a perfect load, since the reflection from its end does not enter the time window over which we measure. This measurement allows us to subtract the background signal superimposed on the reflected voltage pulse. This is necessary since multiple reflections of the voltage pulse at the two ends of the CPW and the T-junction still lead to a distinct signal even after ~400 ps. The resulting voltage pulse $v_{out}(t)$ is plotted in Fig. 3a.

Finally, we calculate the complex reflection coefficient of the coaxial 1.0 mm offset short, $R_{\mathrm{short}}(f)$, using a commercial finite-element simulation tool (CST Microwave Studio) in the time-domain. Metallic losses and the dimensions of the slotted connector are taken into account [23]. The calculated amplitude of the reflection coefficient is shown in Fig. 3b. Due to increasing skin effect losses at higher frequencies, the reflection coefficient decreases from 1 at DC to approximately 0.97 (-0.26 dB) at 300 GHz. Also a small ripple (~60 GHz) can be observed, which results from a resonance between the termination of the short and a small transmission line discontinuity given by the coaxial connection (the offset length of the short is 2.5 mm).

We are now in a situation to estimate $h_{\mathrm{probe}}(t)$ and to evaluate its associated uncertainty using Eq. (4). The uncertainty evaluation is carried out by Monte Carlo calculations as described in Sec. 2. To this end, the estimate $\hat{v}(t_i)$ and the standard deviation $s(\hat{v}(t_i))$ of $v_{in}(t)$ and $v_{out}(t)$ at the individual temporal positions t_i are obtained from six repeated EO measurements. We only consider standard uncertainties here and neglect correlations between different temporal positions of all measured time traces. This is because the estimation of a reliable covariance matrix of a time trace requires a number of measurements on the order of N^2, with N being the number of data points within a measured time trace. For $N = 600$ this is practically impossible. For considerably less than N^2 measurements the resulting covariance matrix would be severely underdetermined and can only be used to extract pulse parameters as shown in Ref. [13]. An approach to address this problem would be to parameterize the structure of the covariance matrix using a limited number of parameters, see outlook. Note that we still take into account correlations

in the output quantity, the impulse response, whose covariance matrix is in general not diagonal due to the model of evaluation. According to [15] we assign a scaled and shifted t-distribution to each measured data point of $v_{in}(t)$ and $v_{out}(t)$, respectively. The scale factor is chosen as $s(\hat{v}(t_i))/\sqrt{5}$ and the shift as $\hat{v}(t_i)$. The PDF assigned to the complete waveform is thus the product of t-distributions. Moreover, to account for possible errors in the calculation of $R_{\mathrm{short}}(f)$, which might result from slightly inaccurate material parameters, we express the magnitude of $R_{\mathrm{short}}(f)$ with the usual definition employing an attenuation constant: $|R_{\mathrm{short}}(f)| = \exp[-\gamma_{\mathrm{short}}\,\alpha_{\mathrm{short}}(f)]$. Here, $\alpha_{\mathrm{short}}(f)$ is the attenuation constant of the MWP and γ_{short} is a dimensionless variable to which we assign a normal distribution with mean 1 and standard deviation of 0.1.

Propagating samples from the (joint) PDF of the input quantities through Eq. (4) and calculating the discrete inverse Fourier transform we obtain samples from the PDF associated with our knowledge about $h_{\mathrm{probe}}(t)$. The estimate of $h_{\mathrm{probe}}(t)$ obtained in this way from 10,000 Monte Carlo runs is shown in Fig. 4a together with two curves denoting the pointwise 95 % coverage intervals. The impulse response of the MWP has a full width at half maximum (FWHM) of 4.1 ps. The ringing with a period of 5 ps is due to an absorption dip in the transfer function of the MWP, which occurs at 200 GHz. Currently we are unsure about the origin of this increased absorption. It has been verified that the ringing is not caused by the Butterworth filter used for regularization. The corresponding covariance matrix derived from the Monte Carlo calculations is plotted in Fig. 4b. The diagonal elements of the matrix correspond to the variances of the time traces, while the off-diagonal elements denote the covariances. As can be clearly seen we obtain correlations around the main peak which have to be taken into account for further calculations.

A more detailed analysis of our result shows that the PDF of $h_{\mathrm{probe}}(t)$ is slightly asymmetric and cannot be approximated with a normal distribution. This is exemplarily shown in the inset of Fig. 4a, in which the histogram of $h_{\mathrm{probe}}(t_{\max})$ is plotted, with $t_{\max}$ being the temporal position of the maximum of the impulse response. Consequently, we directly use the 10,000 Monte Carlo runs of $h_{\mathrm{probe}}(t)$

instead of their mean value and their covariance matrix for further calculations as detailed in the next section.

4) Measurement of the impulse response of the sampling oscilloscope

Having characterized the MWP we now have to determine the other input variables of Eq. (1), namely $v_{osc}(t)$, $v_{eos}(t)$, σ_{osc}, σ_{eos}, and γ_τ, to be able to calculate the impulse response of the oscilloscope:

- The input pulse $v_{in}(t)$ was measured six times at the discrete temporal positions $t_1,\ldots,t_N$ via EO sampling to obtain an estimate and the standard deviation at the individual time instances. As for the MWP we neglect correlations between different temporal positions. Hence, according to [15] a product of scaled and shifted t-distributions was assigned. An example of the corresponding time trace of $v_{in}(t)$ has already been discussed in Sec. 3 and is shown in Fig. 3(a). Again we limit our measurement epoch to a time window of ~100 ps due to the reasons described above.
- The time resolution of the EO measurement technique, σ_{eos}, has been determined using the technique described in Ref. [6] to be $\sigma_{eos}\approx(0.9\pm0.2)$ ps, with 0.2 ps being the standard uncertainty. According to [15] we assigned a normal distribution with mean and standard deviation equal to the estimate and the standard uncertainty of σ_{eos}, respectively.
- The oscilloscope trace $v_{osc}(t)$ was measured ten times by averaging over 512 individual traces; an example of one oscilloscope trace is shown in Fig. 1. From these 10 oscilloscope traces we obtained an estimate of $v_{osc}(t)$ by averaging and the standard deviations at the individual time instances. Similar to our analysis for $v_{in}(t)$ we assign as PDF the product of scaled and shifted t- distributions.
- The oscilloscope jitter σ_{osc} was measured in the statistics mode of the oscilloscope (without averaging) [24]. To this end, the rising edges of 512 oscilloscope traces are analyzed. A frequency distribution is extracted, which shows as a function of time instants how often a value of $V_{max}/2\pm V_{max}/200$ has been measured, with V_{max} being the amplitude of the measured voltage pulse, see Fig. 5. This frequency distribution can be well approximated by a Gaussian distribution with variance σ_{osc}^2. The width of the Gaussian low pass

filter used for the deconvolution of the oscilloscope trace is then given by σ_{osc}^{-2}, see Sec. 2. In principle, voltage noise also contributes to the jitter measurement, however, the effect of noise was found to be negligible. For the 100 GHz oscilloscope under study we measured a remarkably small jitter σ_{osc} = (0.36±0.05) ps, with 0.05 ps being the standard uncertainty. According to [15] we assigned a truncated scaled and shifted t-distribution to σ_{osc} with the shift given by the mean and the scaling determined by the standard deviation of the measurements of σ_{osc}, respectively.

- The time base correction factor γ_τ is defined as $t_{real} = \gamma_\tau\, t_{osci}$ with t_{osci} and t_{real} being the oscilloscope's time base and the corrected time base of the oscilloscope, respectively. In order to determine γ_τ we have measured the repetition rate of our femtosecond laser, f_{rep}, and compared this value to the repetition rate of the voltage pulses measured with the sampling oscilloscope. For the latter measurement we employ a measurement epoch being considerably larger than $1/f_{rep}$. We have verified by changing the delay of the trigger that no abrupt jump in the timebase (see Refs. [25,26]) distorts the measured waveform. However, we also explicitly emphasize that for measurements over longer time windows (of several 100 ps and longer) a more sophisticated time-base correction considering nonlinear distortions as discussed in Refs. [26-28] should be applied. With our technique we obtain a value of γ_τ = 1.00076±0.0002, with 0.0002 being the standard uncertainty. For these measurements the repetition rate of the laser was not stabilized, since the drift of f_{rep} within the measurement time is negligible and does not influence the measurement of γ_τ. According to [15] we assigned a normal distribution with mean and standard deviation equal to the estimate and the standard uncertainty of γ_τ , respectively.

From the model equation (1) we can now estimate the impulse response of the sampling oscilloscope and evaluate the associated uncertainty as described in Section 2. Before obtaining $h_{osc}(t)$ we again perform a regularization of $H_{osc}(f)$ with a 20th order Butterworth filter having a 3dB bandwidth of 190 GHz as extracted from the inset of Fig. 1. We assume the regularization error resulting from the application of the low-pass filter to be negligible. The resulting estimate of $h_{osc}(t)$ employing

10,000 MC runs is depicted in Fig. 6a together with the pointwise 95 % coverage intervals. For the PDF associated with the FWHM of the impulse response the corresponding histogram is plotted in Fig. 6b with a mean value of 4.9 ps and a 95 % coverage interval ranging from 4.6 ps to 5.3 ps. To demonstrate that frequency components above 110 GHz considerably influence the impulse response, we have repeated the same analysis by using a 10^{th} order Butterworth filter with a 3 dB bandwidth of 110 GHz for regularization of $H_{osc}(f)$. The resulting estimate of $h_{osc}(t)$ is plotted in the inset of Fig. 6a together with the estimate obtained from the full model (regularization at 190 GHz). In this case the impulse response is considerably broadened. The histogram of the FWHM of the 10,000 MC runs is plotted in Fig. 6c. A mean value of 5.5 ps and a 95 % coverage interval ranging from 5.3 ps to 5.8 ps are obtained. The mean value is 0.6 ps larger than the resulting value of the full model. Thus, when specifying parameters related to the time-domain response of ultrafast sampling oscilloscopes frequency components above the cut-off frequency of higher-order modes of the coaxial line should be taken into account.

For a full characterization we also visualize in Fig. 6d the covariance matrix for the impulse response shown in Fig. 6a. Again we obtain correlations in the output quantity, which should be taken into account for employing the oscilloscope for high-frequency measurements as shown in recent studies [11,13,29]. However, we do not suggest that mean and covariance matrices are disseminated as part of the calibration process, since they do not fully characterize the obtained distribution. Instead we propose that the resulting Monte Carlo runs of $h_{osc}(t)$ are disseminated. These time traces can then be used for the calculation of individual properties of the sampling oscilloscope that go beyond the parameters presented in this paper.

In a previous study we have characterized a nominal 70 GHz oscilloscope [7] and derived from less sophisticated Monte-Carlo calculations a mean value of the FWHM of the impulse response of (4.2±0.5) ps. At first sight this faster response for the 70 GHz oscilloscope is surprising. However, as verified by an independent study [30] nominal 70 GHz sampling heads might indeed yield faster pulse parameters than nominal 100 GHz sampling heads, most likely, due to an exceptionally good nonlinear transmission line within this particular 70 GHz sampling head. In this regard we like to emphasize again that the measurement of pulse parameters gives

an indication about the speed of the device under test, but is insufficient for a complete characterization.

Finally, we discuss the measurement of the oscilloscope's reflection coefficient. This reflection results from the impedance mismatch between the coaxial waveguide and the sampling circuit of the oscilloscope head and, thus, is also referred to as mismatch [9]. The measurement of this reflection coefficient is important because it determines how the source generating the signal to be measured with the oscilloscope is loaded. This may significantly influence the signal to be measured. In particular, the reflected signal might distort the source and enter the measurement window at later times. In order to measure this reflection coefficient, we use the same setup as described above: The oscilloscope head is connected to the MWP, which, in turn, is attached to the CPW. The voltage pulse propagating into the MWP is then measured at the T-junction over a long time window of ~450 ps. This time window not only includes the voltage pulse traveling towards the sampling head, but also the one being reflected from the sampling head and traveling backwards. The reflection is superimposed on a background signal as discussed in Sec. 3. We again connect a long coaxial cable to the end of the MWP to measure the background signal and extract the reflected pulse, $v_{\mathrm{r,osci}}(t)$. This pulse is plotted in Fig. 7 together with the reflection obtained from the coaxial short, $v_{\mathrm{r,short}}(t)$, which is similar to the curve plotted in Fig. 3. As can be seen in Fig. 7 the reflection from the sampling circuit of the oscilloscope appears ~280 ps later than the one from the coaxial short. These two time traces and the calculated reflection coefficient of the short allow us to derive the complex reflection coefficient of the sampling head from

$$R_{\mathrm{osc}}(f) = \frac{V_{\mathrm{r,osc}}(f)}{V_{\mathrm{r,short}}(f)} R_{\mathrm{short}}(f) \ . \tag{5}$$

Again, we used 10,000 Monte Carlo runs to derive a estimate of $R_{\mathrm{osc}}(f)$ and its corresponding uncertainty. The magnitude of the estimate of the reflection coefficient is plotted in the inset of Fig. 8a together with the corresponding 95 % confidence intervals. Remarkably, $|R_{\mathrm{osc}}(f)|$ is larger than 0.5 around 80 GHz and decreases at larger frequencies. Additional measurements are necessary to investigate this behavior in more detail. In particular it will be interesting to see

whether this behavior can be found for other sampling heads, too. After an inverse Fourier transform of $R_{osc}(f)$ we obtain the impulse response $r_{osc}(t)$ of the reflection, whose estimate and corresponding 95 % pointwise coverage intervals are plotted in Fig. 8a. To complete the uncertainty evaluation we also plot the corresponding covariance matrix in Fig. 8b, visualizing the correlations in the time domain.

5. Conclusions and outlook

In summary, we employed optoelectronic techniques based on femtosecond lasers to measure the impulse response of a 1.0 mm microwave probe and a 100 GHz sampling oscilloscope including the oscilloscope mismatch within a ~100 ps time window. Our measurement technique also captures the response of these devices above 110 GHz which is the cut-off frequency of higher-order modes of the 1.0 mm coaxial line. The uncertainty evaluation has been performed by employing a Monte Carlo method according to the Supplement 1 to the GUM, and we determined correlations in the estimated impulse responses, which arise from the analytical model.

Future studies will concentrate on extending the measurement epoch and, thus, allow for a characterization at reduced frequencies. This will enable a detailed comparison with scalar techniques for the oscilloscope characterization, as discussed in Refs. [9,31]. Moreover, it will be interesting to see whether a parametric description of the covariance structure of the measured time traces is possible. If the number of parameters needed for an accurate description is smaller than the number of measurements, this approach will allow us to consider correlations in the measured time traces, as well.

Acknowledgements

We thank LeCroy Europe GmbH for the loan of a 100 GHz sampling head and B. Hacke and H. Mary for expert technical assistance. Moreover, we thank the reviewers of this manuscript for their fruitful comments.

References

[1] H.C. Reader, D.F. Williams, P.D. Hale, and T.S. Clement, "Comb-Generator Characterization," *Microwave Theory and Techniques, IEEE Transactions on*, vol. 56, 2008, pp. 515-521.

[2] D. Williams, P. Hale, and K.A. Remley, "The Sampling Oscilloscope as a Microwave Instrument," *IEEE Microwave Magazine*, vol. 8, Aug. 2007, pp. 59-68.

[3] D.A. Humphreys, M.R. Harper, and M. Salter, "Traceable calibration of Vector Signal Analyzers," *Microwave Measurements Conference (ARFTG), 2010 75th ARFTG*, Anaheim: 2010, pp. 1-4.

[4] G. Breed, "Analyzing signals using the eye diagram," *High Frequency Electronics*, vol. 11, 2005, pp. 50-52.

[5] W.J. Dally and J.W. Poulton, "Digital systems engineering," *Cambridge University Press*, 1998.

[6] M. Bieler, K. Pierz, and U. Siegner, "Simultaneous generation and detection of ultrashort voltage pulses in low-temperature grown GaAs with below-bandgap laser pulses," *Applied Physics Letters*, vol. 94, Feb. 2009, pp. 051108-3.

[7] M. Bieler, M. Spitzer, K. Pierz, and U. Siegner, "Improved Optoelectronic Technique for the Time-Domain Characterization of Sampling Oscilloscopes," *IEEE Transactions on Instrumentation and Measurement*, vol. 58, 2009, pp. 1065-1071.

[8] M. Harper, A. Smith, A. Basu, and D. Humphreys, "Calibration of a 70 GHz Oscilloscope," *2004 Conference on Precision Electromagnetic Measurements*, IEEE, 2004, pp. 530-531.

[9] T.S. Clement, P.D. Hale, D.F. Williams, C.M. Wang, A. Dienstfrey, and D.A. Keenan, "Calibration of sampling oscilloscopes with high-speed photodiodes," *IEEE Transactions on Microwave Theory and Techniques*, vol. 54, 2006, pp. 3173-3181.

[10] M. Bieler, S. Seitz, M. Spitzer, G. Hein, K. Pierz, U. Siegner, M.A. Basu, A.J.A. Smith, and M.R. Harper, "Rise-Time Calibration of 50-GHz Sampling Oscilloscopes: Intercomparison Between PTB and NPL," *IEEE Transactions on Instrumentation and Measurement*, vol. 56, 2007, pp. 266-270.

[11] D.F. Williams, A. Lewandowski, T.S. Clement, J.C.M. Wang, P.D. Hale, J.M. Morgan, D.A. Keenan, and A. Dienstfrey, "Covariance-based uncertainty analysis of the NIST electrooptic sampling system," *IEEE*

Transactions on Microwave Theory and Techniques, vol. 54, Jan. 2006, pp. 481-491.

[12] D.F. Williams, P.D. Hale, T.S. Clement, and J.M. Morgan, "Calibrated 200-GHz waveform measurement," *IEEE Transactions on Microwave Theory and Techniques*, vol. 53, Apr. 2005, pp. 1384-1389.

[13] P.D. Hale, A. Dienstfrey, J. Wang, D.F. Williams, A. Lewandowski, D.A. Keenan, and T.S. Clement, "Traceable Waveform Calibration With a Covariance-Based Uncertainty Analysis," *IEEE Transactions on Instrumentation and Measurement*, vol. 58, Oct. 2009, pp. 3554-3568.

[14] A. Dienstfrey, P.D. Hale, D.A. Keenan, T.S. Clement, and D.F. Williams, "Minimum-phase calibration of sampling oscilloscopes," *IEEE Transactions on Microwave Theory and Techniques*, vol. 54, 2006, pp. 3197-3208.

[15] "Supplement 1 to the 'Guide to the expression of uncertainty in measurement' —Propagation of distributions using a Monte Carlo method," Bureau International des Poids et Mesures, 2008.

[16] S. Seitz, M. Bieler, M. Spitzer, K. Pierz, G. Hein, and U. Siegner, "Optoelectronic measurement of the transfer function and time response of a 70 GHz sampling oscilloscope," *Measurement Science and Technology*, vol. 16, Oct. 2005, pp. 7-9.

[17] M. Bieler, M. Spitzer, G. Hein, U. Siegner, F. Schnieder, T. Tischler, and W. Heinrich, "Broadband characterization of a microwave probe for picosecond electrical pulse measurements," *Measurement Science and Technology*, vol. 15, Sep. 2004, pp. 1694-1701.

[18] *A 1.0 mm adapter has been connected to the sampling head to protect its coaxial connector during the measurements. For the following analysis the adaptor is assumed to be part of the sampling head. Similarly, due to experimental reasons, a male-male adaptor has been connected to the coaxial end of the MWP and is assumed to be part of the MWP.*

[19] *For a tutorial on the analysis in the time domain together with an uncertainty evaluation in line with GUM/GUM-S1 we refer the reader to* C. Elster and A. Link, "Uncertainty evaluation for dynamic measurements modelled by a linear time-invariant system." *Metrologia*, vol. 45, 2008, pp. 464-473, S. Eichstädt, C. Elster, T. J. Esward and J. P. Hessling, "Deconvolution filters for the analysis of dynamic measurement processes: a tutorial." *Metrologia*, 2010, vol. 47, 522-533.

[20] J. Verspecht, "Compensation of timing jitter-induced distortion of sampled waveforms," *IEEE Transactions on Instrumentation and Measurement*, vol. 43, 1994, pp. 726-732.

[21] S.M. Riad, "The deconvolution problem: An overview," *Proceedings of the IEEE*, vol. 74, 1986, pp. 82-85.

[22] M. Bieler, "Transfer of sub-5 ps electrical test pulses to coplanar and coaxial electronic devices," *Electronic Letters*, vol. 38, 2002, pp. 125-126.

[23] *Rosenberger, private communication.*

[24] M. Bieler, M. Spitzer, G. Hein, U. Siegner, and E.O. Göbel, "Ultrafast optics establishes metrological standards in high-frequency electronics," *Applied Physics A: Materials Science & Processing*, vol. 78, Mar. 2004, pp. 429-433.

[25] G. Vandersteen, Y. Rolain, and J. Schoukens, "An identification technique for data acquisition characterization in the presence of nonlinear distortions and time base distortions," *IEEE Transactions on Instrumentation and Measurement*, vol. 50, 2001, pp. 1355-1363.

[26] F. Verbeyst, "Contributions to large-signal network analysis," *PhD Thesis, Vrije Universiteit Brussel*, 2006.

[27] P.D. Hale, C.M. Wang, D.F. Williams, K.A. Remley, and J.D. Wepman, "Compensation of Random and Systematic Timing Errors in Sampling Oscilloscopes," *IEEE Transactions on Instrumentation and Measurement*, vol. 55, Dec. 2006, pp. 2146-2154.

[28] J.A. Jargon, P.D. Hale, and C.M. Wang, "Correcting Sampling Oscilloscope Timebase Errors With a Passively Mode-Locked Laser Phase Locked to a Microwave Oscillator," *IEEE Transactions on Instrumentation and Measurement*, vol. 59, Apr. 2010, pp. 916-922.

[29] S. Eichstädt, A. Link, M. Spitzer, M. Bieler, and C. Elster, "Significance of correlation in the unvertainty evaluation of sampling oscilloscope measurements," *imeko2009.it.pt*, 2009, pp. 476-479.

[30] J.R. Andrews, "Comparison of Ultra-Fast Risetime Sampling Oscilloscopes," *Application Note AN-2e, www.picosecond.com/objects/AN-02e.pdf*, 2011.

[31] D.F. Williams, T.S. Clement, K.A. Remley, P.D. Hale, and F. Verbeyst, "Systematic Error of the Nose-to-Nose Sampling-Oscilloscope Calibration," *IEEE Transactions on Microwave Theory and Techniques*, vol. 55, Sep. 2007, pp. 1951-1957.

Figure 1

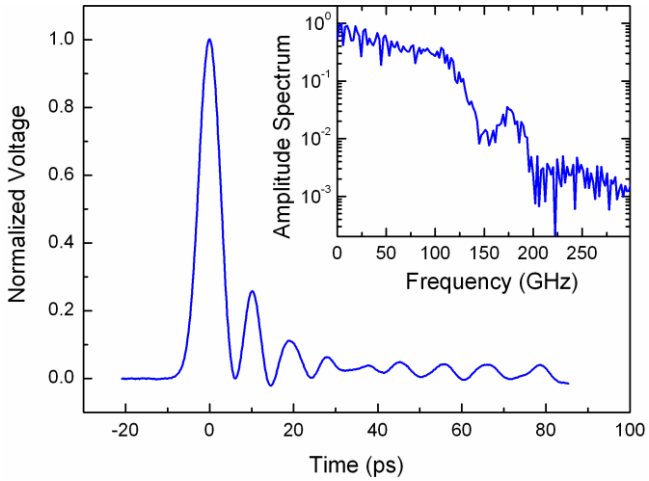

Measured oscilloscope trace of an ultrashort voltage pulse generated with optoelectronic techniques. Shown are the first 100 ps out of a 500 ps measurement epoch. The pulse has a full width at half maximum of 5.9 ps. The spectrum of the 500 ps long time trace is shown in the inset. The measured pulse contains spectral components up to ~190 GHz.

Figure 2

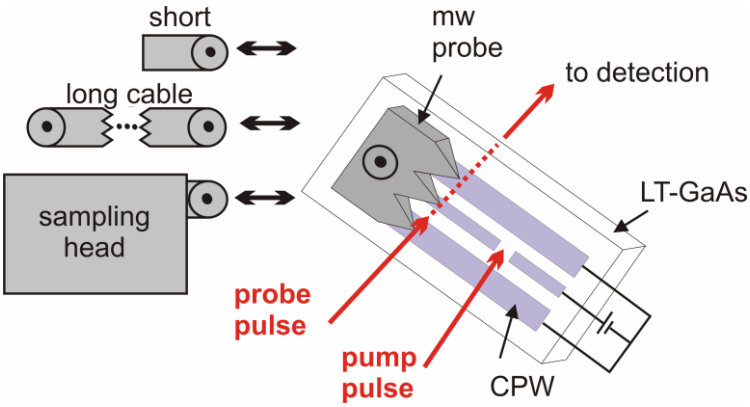

Schematic view of the optoelectronic experimental set-up. The CPW on top of the LT-GaAs substrate incorporates a PCS, which is biased with 20 V. Optical pump pulses with a length of ~150 fs are focused on the gap of the PCS to generate ultrashort voltage pulses, which can be detected using standard EO techniques in transmission geometry. A MWP is used for the transfer of the ultrashort voltage pulses to a 1.0 mm coaxial line.

Figure 3

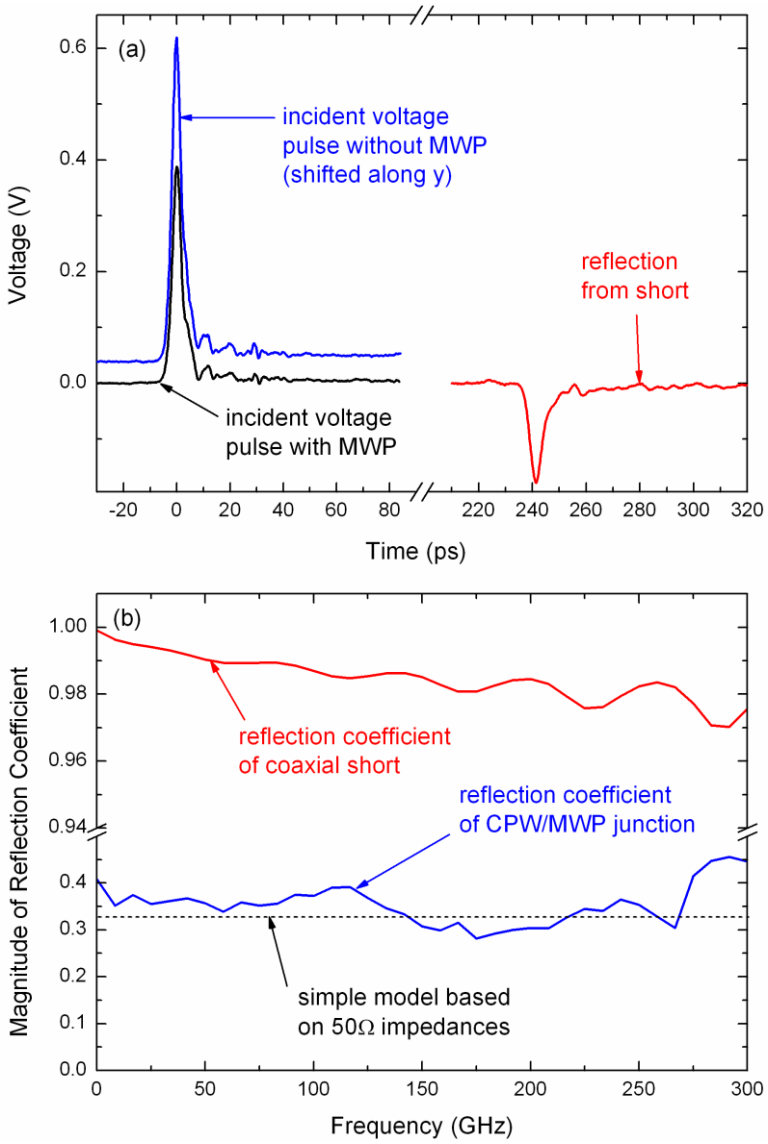

(a) Voltage pulse measured electro-optically at the position where the MWP is attached to the CPW. Black line: with attached MWP, blue line: with MWP lifted off the CPW, red line: voltage pulse back reflected from the coaxial offset short. The voltage pulses measured with and without attached MWP both have a FWHM of 4.0 ps. (b) Measured amplitude of the reflection coefficient of the T-junction (blue line) and calculated amplitude of the reflection coefficient of the coaxial offset short (red line).

Figure 4

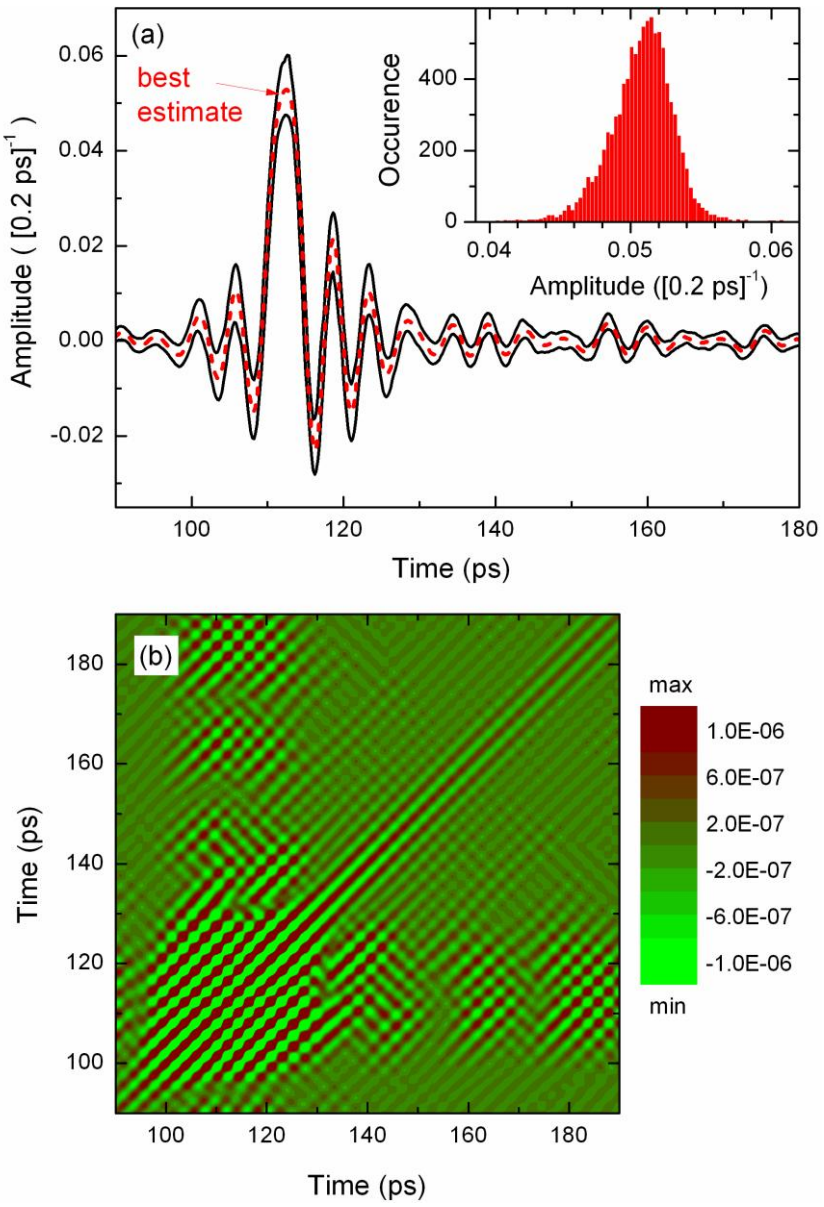

(a) Estimate (red dashed line) of the impulse response of the 1.0 mm MWP with pointwise 95 % coverage intervals (black solid lines). The inset shows a histogram of the maximum value of the impulse response obtained from 10,000 MC runs. (b) Covariance matrix of the impulse response of the MWP obtained from the MC method. The off-diagonal elements denote the covariances in the time trace.

Figure5

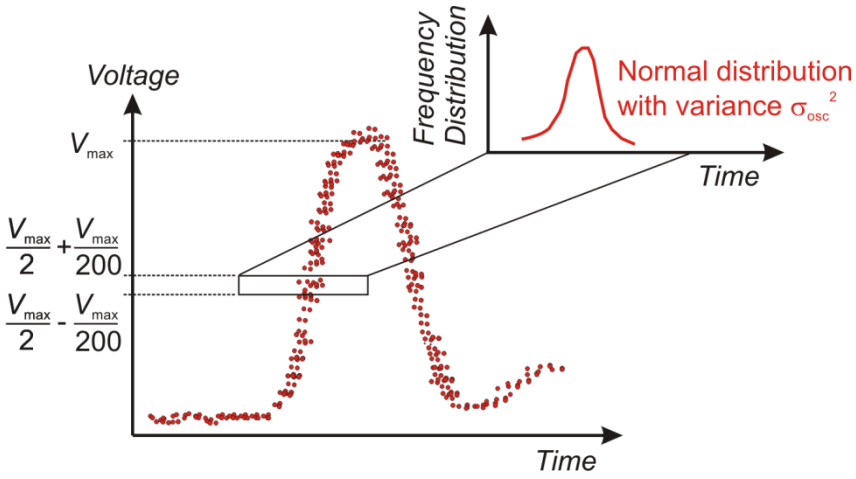

Schematic illustration of the jitter measurement.

Figure 6

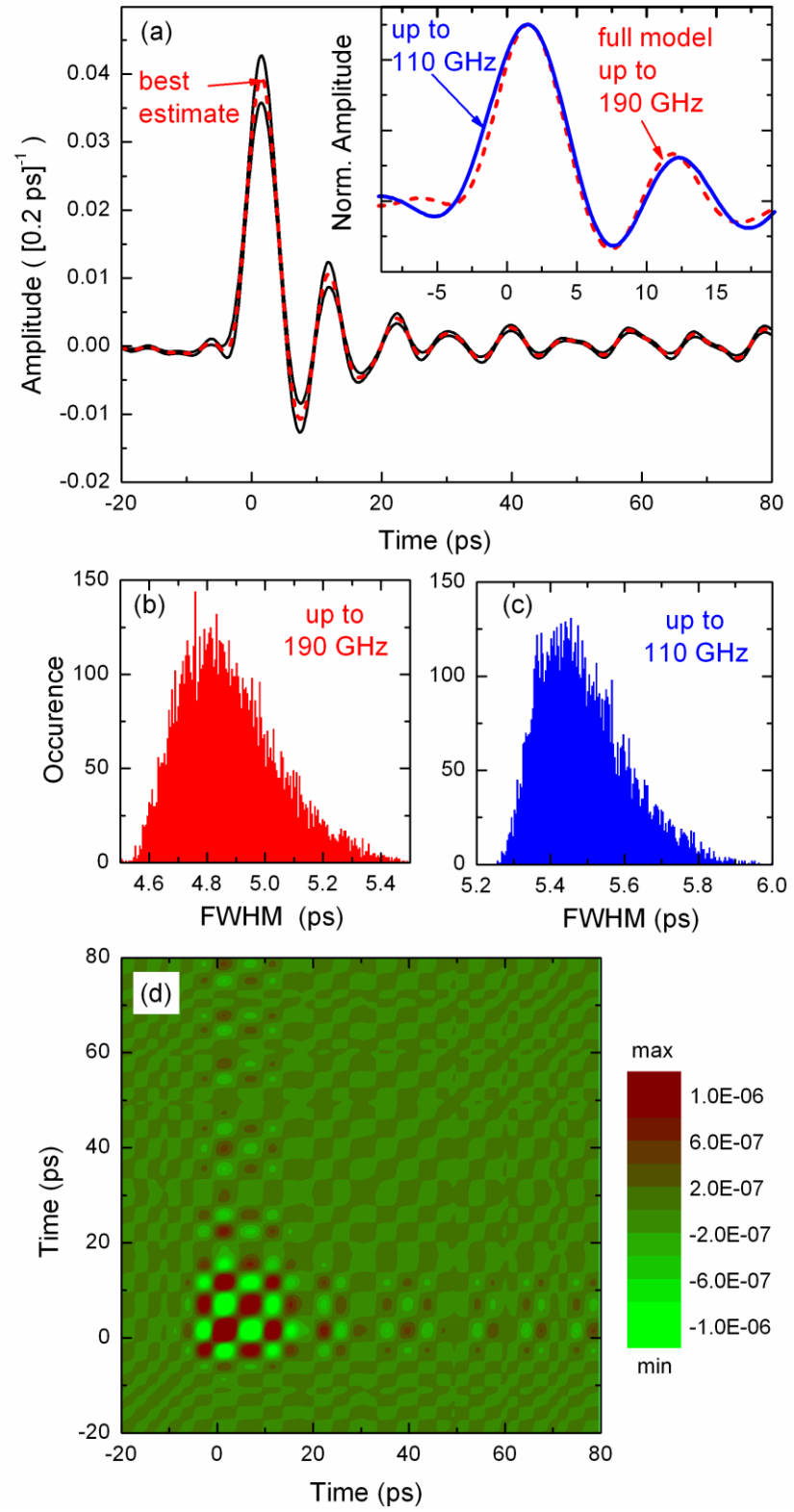
(a)
best
estimate
up to
110 GHz
full model
up to
190 GHz
Norm. Amplitude
Amplitude ([0.2 ps]$^{-1}$)
Time (ps)
(b)
up to
190 GHz
Occurence
FWHM (ps)
(c)
up to
110 GHz
FWHM (ps)
(d)
Time (ps)
Time (ps)
max
1.0E-06
6.0E-07
2.0E-07
-2.0E-07
-6.0E-07
-1.0E-06
min

(a) Estimate (red dashed line) of the impulse response of the 100 GHz sampling head with pointwise 95 % coverage intervals (black solid lines). The inset shows the estimate plotted in (a) together with the estimate obtained by considering only frequencies up to 110 GHz. (b) Histogram of the FWHM of the impulse response obtained from 10,000 MC runs for the full model. (c) Histogram of the FWHM of the impulse response obtained from 10,000 MC runs considering frequencies up to 110 GHz. (d) Covariance matrix of the impulse response of the sampling head obtained from the MC simulations.

Figure 7

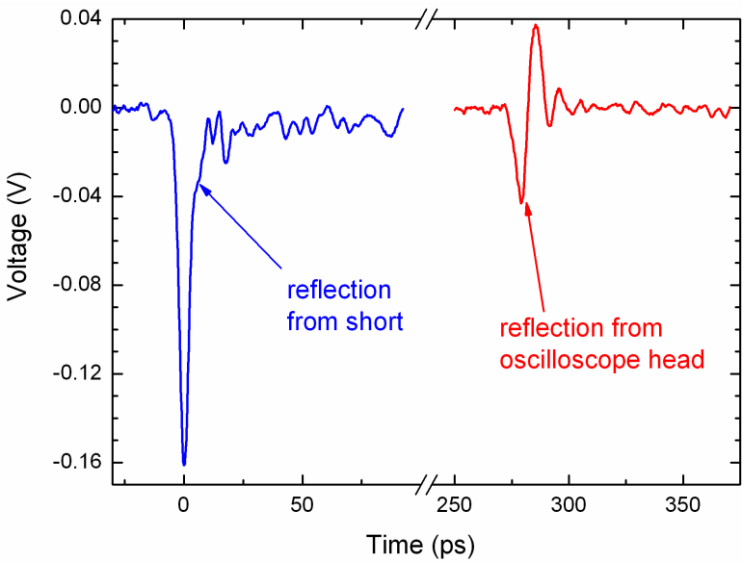

Electro-optically measured voltage pulse at the T-junction that is back reflected from the coaxial offset short (blue line) and back reflected from the oscilloscope head (red line).

Figure 8

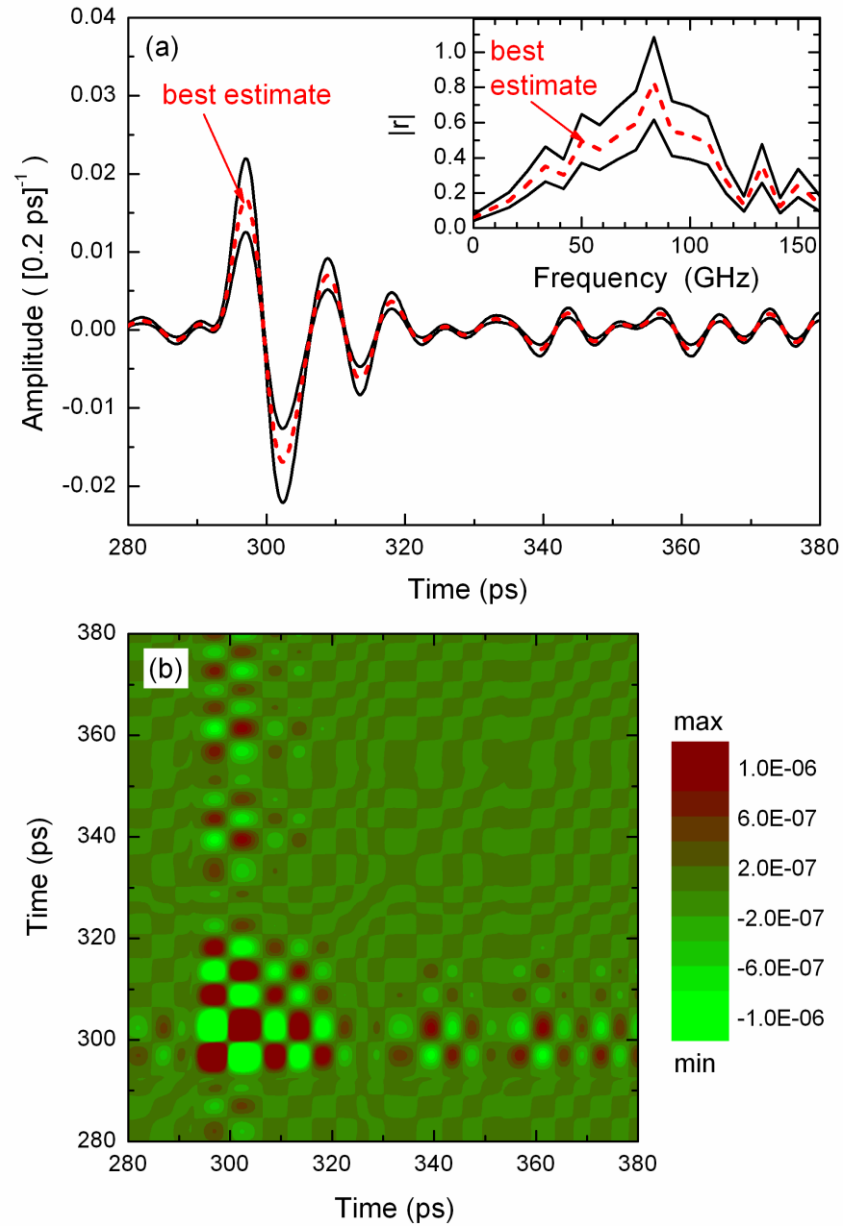

(a) Estimate (red dashed line) of the impulse response of the oscilloscope reflection with pointwise 95 % coverage intervals (black solid lines). The inset depicts the corresponding reflection coefficient in the frequency domain, which is larger than

0.5 for frequencies around 80 GHz. (b) Covariance matrix of the time –domain trace plotted in (a) obtained from the MC simulations..